Scanning gate imaging of two coupled quantum dots in single-walled carbon nanotubes

2014 Nanotechnology 25 495703

(http://iopscience.iop.org/0957-4484/25/49/495703)

IOP Publishing Nanotechnology
Nanotechnology **25** (2014) 495703 (8pp) doi:10.1088/0957-4484/25/49/495703

Scanning gate imaging of two coupled quantum dots in single-walled carbon nanotubes

Xin Zhou[1], James Hedberg[2], Yoichi Miyahara[2], Peter Grutter[2] and Koji Ishibashi[1]

[1] Advanced Device Laboratory and Center for Emergent Matter Science (CEMS), RIKEN, 2-1 Hirosawa, Wako, Saitama 351-0198, Japan
[2] Department of Physics, McGill University, 3600 rue University, Montreal, Quebec, H3A 2T8, Canada

E-mail: xzhounj@gmail.com and yoichi.miyahara@mcgill.ca

Received 12 May 2014, revised 16 July 2014
Accepted for publication 16 October 2014
Published 21 November 2014

Abstract

Two coupled single wall carbon nanotube quantum dots in a multiple quantum dot system were characterized by using a low temperature scanning gate microscopy (SGM) technique, at a temperature of 170 mK. The locations of single wall carbon nanotube quantum dots were identified by taking the conductance images of a single wall carbon nanotube contacted by two metallic electrodes. The single electron transport through single wall carbon nanotube multiple quantum dots has been observed by varying either the position or voltage bias of a conductive atomic force microscopy tip. Clear hexagonal patterns were observed in the region of the conductance images where only two sets of overlapping conductance rings are visible. The values of coupling capacitance over the total capacitance of the two dots, $C_m/C_{1(2)}$ have been extracted to be 0.21 ~ 0.27 and 0.23 ~ 0.28, respectively. In addition, the interdot coupling (conductance peak splitting) has also been confirmed in both conductance image measurement and current–voltage curves. The results show that a SGM technique enables spectroscopic investigation of coupled quantum dots even in the presence of unexpected multiple quantum dots.

Keywords: carbon nanotube quantum dots, scanning gate microscopy, Coulomb blockade, single-electron tunneling

(Some figures may appear in colour only in the online journal)

1. Introduction

Single-walled carbon nanotubes (SWCNTs), as one of the promising one dimensional semiconductor materials, offer the opportunity to investigate quantum-dot (QD) systems [1]. Both single electron charging effects and energy level quantization in SWCNT–QDs can be observed at relatively high temperature due to their extremely small diameter (about 1 nm). SWCNT–QDs based quantum computing devices are also very promising due to the suppression of the large-angle scatterings and long range Coulomb scatterings [2]. SWCNT–QDs have revealed interesting physics, such as Zeeman splitting, Kondo effect, electron-hole symmetry, four- or two-electron shell filling phenomenon and so on [3–5].

Well-defined SWCNT–QDs can be obtained with conventional lithography techniques by depositing metallic contacts on top of an individual SWCNT. However, when we fabricate QDs in SWCNT with lithographically defined electrodes, unexpected multiple-dots are often formed due to accidentally induced defects [6]. Investigation of those defect-induced QDs is a great challenge for lithographically defined gates because the spatial locations of these dots are unknown.

Recently, this obstacle has been overcome by scanning gate microscopy (SGM) technique, which uses a conducting atomic force microscopy (AFM) tip as a movable gate to scan over the QDs while measuring the conductance through the QDs. The resulting conductance images of QDs show concentric rings (Coulomb rings) around the center of the QD,

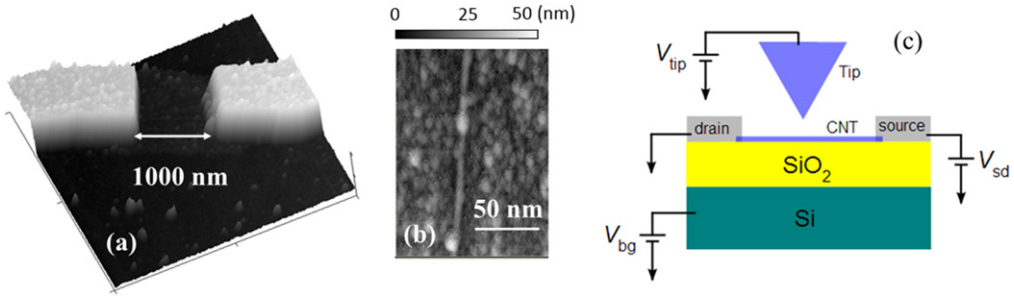

Figure 1. (a) AFM topography image of the device structure with 1000 nm contact gap. (b) AFM topography image of SWCNT channel obtained by zoom in scanning of the channel area of figure 1(a). All AFM images were taken by the home-built AFM at a temperature of 170 mK. (c) Schematic of experimental setup.

each of which corresponds to a single-electron charging event and thus allows us to identify the locations of these QDs [7–9]. Here, we show our experimental results on two coupled QDs in SWCNT multiple QD system by taking advantage of the low temperature SGM technique. Experimental results show that single-electron transport in double quantum dots can be investigated by moving the AFM tip as a local gate even in the presence of defect-induced multiple QDs. In addition, we also observed the CB peak splitting phenomenon in two coupled QDs.

2. Experimental

The device was fabricated on a highly doped Si substrate capped with a 200 nm thick silicon dioxide layer. Well-aligned SWCNT arrays, which were grown on quartz substrates by the thermal chemical vapor deposition method, were transferred to SiO_2 substrates by taking advantage of the transfer-printed technique [10, 11]. The SWCNT channel was formed by depositing 60 nm thick titanium source–drain contacts with the electron beam evaporator and subsequent lift-off process. The distance between source and drain contacts is 1 μm. The highly doped Si substrate is used as a global back-gate by applying a backgate voltage (V_{bg}). A home-built AFM with a quartz tuning fork force sensor is used to image electrical conduction through the SWCNT, at a temperature of 170 mK [12]. During SGM measurements, an electrochemically etched tungsten tip is scanned in a plane about 55 nm above the SWCNT. Figure 1(a) shows an AFM topography image of the device structure with 1 μm contact gap, measured by this home-built AFM at a temperature of 170 mK with frequency modulation mode using a phase-locked loop oscillation controller (SPECS OC4) and an open source SPM controller (SoftdB MK2-A810) together with the GXSM software [13] . The SWCNT channel can be observed clearly in the AFM image, as shown in figure 1(b). The roughness of the topography around the SWCNT is due to the residue of the resist used during the fabrication process. A simple schematic of experimental setup was shown in figure 1(c). The dc voltage source, for biasing drain–source voltage V_{ds}, was followed with a resistor and also a low pass filter in series before connecting to the device in the fridge. In the following, the values of V_{ds} all correspond to the values which are setted on the voltage source at room temperature.

3. Results and discussion

3.1. Tip and back gate bias spectroscopy

Characterization was started by measuring standard current–gate voltage (I–V) curves through source–drain contacts. The drain–source current (I_{ds}) versus gate voltage curves were measured by biasing V_{ds} to be 5 mV and sweeping either V_{bg} or tip voltage (V_{tip}). The results are shown in figures 2(a) and (c), respectively. In these measurement, the AFM tip is located near the center of the SWCNT channel 10 nm above the SWCNT. Clear Coulomb blockade (CB) oscillations have been observed in both curves. Thus, when the tip is placed at a fixed position over SWCNT-dots, it has the similar function as the backgate which gates globally the single-electron transport. In the case of vanishing single-particle energy level spacing, the period of CB oscillations in gate voltage, ΔV_{gate}, corresponds to a change of a single electron and is described by: $\Delta V_{gate} = e/C_{gate}$, where e is the elementary charge and C_{gate} is the capacitance between dot and gate [14]. For a single dot, CB oscillations exhibit uniform oscillations for V_{gate} because the C_{gate} is constant and unique in the system. When a single electron passes through multiple QDs, CB oscillations exhibit irregular oscillations due to the variations of C_{gate} for each different QD and also the coupling effects between neighboring QDs [11]. Thus, these irregular Coulomb oscillations (as shown in figures 2(a) and (c)) indicate that the unexpected multiple QDs were formed in this SWCNT channel. The formation of those multiple QDs may be due to the defects in CNTs which were induced during the complicate fabrication processes or SWCNT growth process [6, 15]. When these defects act as strong electron scatterers, QDs were formed between each two defects. The electron scattering effects by defects can be minimized by gate modulation on local fermi level of SWCNT. Consequently, QDs which are formed by these defects exhibit gate-tunable characteristics [16]. Figures 2(a) and (c) exhibit quite different CB oscillations. The backgate plays a global role by modulating all QDs which are formed by unexpected defects along SWCNT

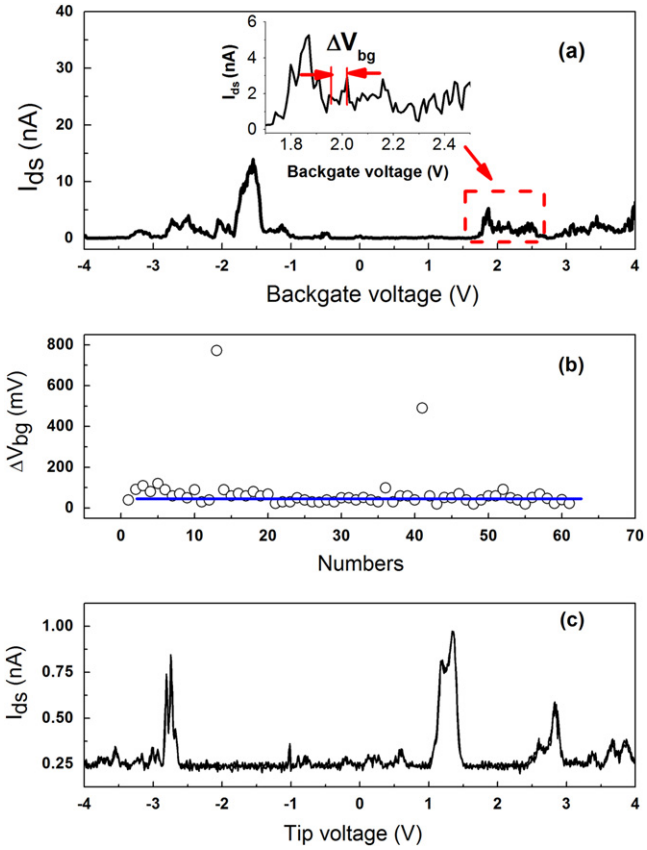

Figure 2. $I_{ds}-V_{bg}$ characteristics measured by biasing $V_{ds} = 5$ mV and the inset shows the zoom in $I_{ds}-V_{bg}$ characteristics in the range from $V_{bg} = 1.7$ to 2.5 V. (b) Variations of distance between nearest neighbor Coulomb peaks V_{bg} versus counting numbers. Here, values of Vbg were taken by zooming in the $I_{ds}-V_{bg}$ characteristics in (a), in the two ranges from $V_{bg} = -2.86$ to -0.38 V and $V_{bg} = 1.70$ to 3.98 V. (c) $I_{ds}-V_{tip}$ characteristics, measured by biasing $V_{ds} = 5$ mV and locating AFM tip near the center of device channel.

channel as well as the Schottky barrier formed at both Ti/SWCNT contacts, whereas the AFM tip acts as a local and movable gate. The modulation of chemical potential of each SWCNT–QD and tunnel barriers by the AFM tip is highlydependent on the distance between the tip and QDs because the capacitance between the tip and each SWCNT–QD, $C_{dot-tip}(\boldsymbol{r}_{tip}, \boldsymbol{r}_{dot})$, is a function of the positions of the tip and each dot, where $\boldsymbol{r}_{tip}$ and $\boldsymbol{r}_{dot}$ are the positions of the tip and QD, respectively. Consequently, SWCNT–QDs exhibit different CB oscillation curves when they are modulated by either V_{tip} or V_{bg}. In order to estimate the sizes of these unexpected SWCNT–QDs, the voltage difference between each two nearest CB peaks ΔV_{bg} (shown in figure 2(a)) versus the number of peaks (corresponding to the number of electrons) is plotted in figure 2(b). These numbers correspond to count the charging event numbers when a single electron overcomes charging energy and tunnels through these multi-QDs [9]. The average values of ΔV_{bg} is 70 mV. The length of these unexpected SWCNT–QDs (l_{dot}) were evaluated by using the formula: $C_{bg} = 2\epsilon_r\epsilon_0 l_{dot}/\ln(2d/a)$ [17] together

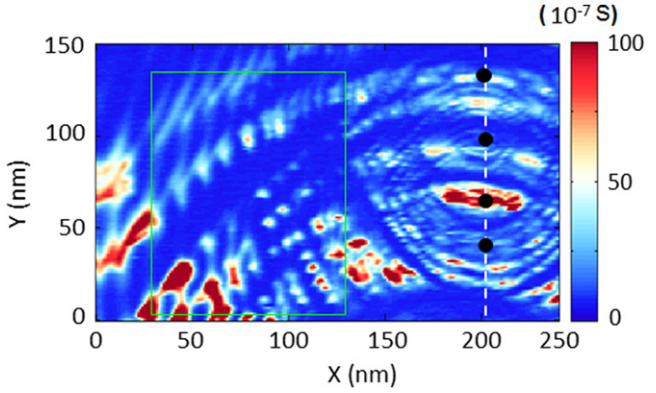

Figure 3. Conductance image over the SWCNT with $V_{tip} = -2.3$ V, $V_{bg} = -10$ mV and $V_{ds} = 4$ mV. The tip is scanned in a plane 10 nm above the surface on which the SWCNT channel exists. The scanning range is $\Delta X_{tip} = 250$ nm and $\Delta Y_{tip} = 150$ nm. Several SWCNT QDs were found along the SWCNT (white dashed line) and marked with dark points. The region enclosed with the green rectangle corresponds to the images shown in figure 4.

with the relation, $\Delta V_{bg} = e/C_{bg}$. Here, C_{bg} is the backgate—SWCNT capacitance, a the radius of SWCNT, d the thickness of the insulator SiO_2, ϵ_r the dielectric constant of SiO_2. The radius of SWCNT is around 1 nm which fulfills the conditions $a \ll d$ for this logarithmic form formula to be valid. Based on the average values of ΔV_{bg} 70 mV, the corresponding length of SWCNT–QDs was deduced to be 57 nm, which is much smaller than the SWCNT channel length (1 μm) defined by the distance between source and drain contacts. Here, the measurement results of $I_{ds} - V_{tip}$ shown in figure 2(c) were not used to evaluate the length of SWCNT–QDs because the $I_{ds} - V_{tip}$ curves are highly dependent on the tip position and no analytical formula is available for the tip—SWCNT capacitance.

3.2. SGM imaging

The conductance images of SWCNT were obtained by scanning the AFM tip above the SWCNT channel as a movable gate. Figure 3 shows the differential conductance dI_{ds}/V_{ds} versus tip position X_{tip} and Y_{tip} which were measured by fixing tip voltage $V_{tip} = -2.3$ V, $V_{ds} = 4$ mV and $V_{bg} = -10$ mV with standard lock-in technique. Several sets of concentric overlapping rings have been observed which are due to the existence of the multiple-QDs connected in series along the length of the SWCNT between source–drain contacts. Each conductance ring corresponds to a Coulomb conductance peak of the quantum dots shown in figure 2(c). These conductance rings are centered over each SWCNT–QD [18–20]. Based on this principle, the location of both SWCNT and SWCNT–QDs were marked with the white dash line and black points respectively, as shown in figure 3. We can understand the working principle of scanning gate conductance imaging by considering the electrochemical potential of the Nth electron in the QD, μ^N_{QD} due to the position dependent tip–dot coupling capacitance, $C_{dot-tip}(\boldsymbol{r}_{tip}, \boldsymbol{r}_{dot})$

such as

$$\mu_{\mathrm{QD}}^{N} = \frac{e^2}{C_\Sigma}\left(N - \frac{1}{2}\right) - \frac{e}{C_\Sigma}\left\{C_{\mathrm{dot-tip}}\left(\boldsymbol{r}_{\mathrm{tip}}, \boldsymbol{r}_{\mathrm{dot}}\right)V_{\mathrm{tip}} + C_{\mathrm{bg}}V_{\mathrm{bg}}\right\}, \quad (1)$$

where C_Σ is the total capacitance of the QD [20].

The electrochemical potential of the QD can be controlled either by varying V_{tip} or by varying $C_{\mathrm{dot-tip}}(\boldsymbol{r}_{\mathrm{tip}}, \boldsymbol{r}_{\mathrm{dot}})$. When the tip is scanned with a constant bias V_{tip}, the chemical potential of SWCNT–QDs moves in or out of the transport window by varying coupling capacitance $C_{\mathrm{dot-tip}}(\boldsymbol{r}_{\mathrm{tip}}, \boldsymbol{r}_{\mathrm{dot}})$ through varying tip position, $\boldsymbol{r}_{\mathrm{tip}}$. When the chemical potential of the QD is aligned with those of source and drain electrodes at certain tip positions, an increased conductance is observed. If $C_{\mathrm{dot-tip}}(\boldsymbol{r}_{\mathrm{tip}}, \boldsymbol{r}_{\mathrm{dot}})$ is just a function of the distance between the QD and the tip position, e.g. $C_{\mathrm{dot-tip}}(\boldsymbol{r}_{\mathrm{tip}}, \boldsymbol{r}_{\mathrm{dot}}) = C_{\mathrm{dot-tip}}(\left|\boldsymbol{r}_{\mathrm{tip}} - \boldsymbol{r}_{\mathrm{dot}}\right|)$, the positions with increased conductance form a circular ring (conductance ring). The geometry of these conductance rings depends on many factors, such as geometry of quantum dots, the coupling capacitance between AFM-tip and source-drain electrodes, and so on. In the previous reports, the CB conductance rings of lithographically defined QDs measured by SGM usually exhibit distorted circular shape [18, 20–23]. For QDs formed in nanotubes or wires, the conductance rings show elliptical shape. When the quantum dot is longer than the tip to nanotube or nanowire distance, the conductance rings will be stretched along the nanotube or nanowire [9, 24], which is caused by the elongated shape of the electron confinement potential profile.

In order to characterize the single-electron transport in two SWCNT–QDs, we focus on the region of the conductance image where only two sets of overlapping rings are visible. This region is indicated with the green rectangle, marked in figure 3. The tip is scanned in a plane 55 nm above the sample surface in a range of $\Delta X_{\mathrm{tip}} = 100$ nm and $\Delta Y_{\mathrm{tip}} = 130$ nm. The evolution of the two sets of conductance rings which correspond to dot1 and dot2 are tracked in a series of SGM conductance images taken at various V_{bg} ranging from −40 to 0 mV with 5 mV step while keeping $V_{\mathrm{ds}} = 4$ mV and $V_{\mathrm{tip}} = -2.1$ V constant. The results are shown in figures 4(a)–(i). Each time the tip crosses a ring toward its center, one electron is pushed out of the QD with the negatively biased tip. As can be seen from equation (1), when V_{bg} increases toward more positive value, the electrochemical potential of the QD is lowered by $eC_{\mathrm{bg}}V_{\mathrm{bg}}/C_\Sigma$ with respect to those of source and drain electrode, requiring this amount to be compensated by increasing $eC_{\mathrm{dot-tip}}V_{\mathrm{tip}}/C_\Sigma$. As V_{tip} is kept constant during SGM scan, increasing $eC_{\mathrm{dot-tip}}V_{\mathrm{tip}}/C_\Sigma$ requires a larger $C_{\mathrm{dot-tip}}$. This causes conductance rings to shrink into the center of the dot with increasing V_{bg} as shown in figures 4(a)–(i).

As shown in figure 4(a), the two sets of conductance rings form hexagonal patterns which resemble the charge stability diagram typically observed in double quantum dot devices. The conductance rings show a split at each intersection. Each of the conductance rings that belong to two dots are marked with green and black lines, respectively. As in the case with the single-electron transport in double-dot system, conductance rings are formed when the energy levels of two dots move into the transport bias window defined by V_{ds}. The split sections of the conductance rings were connected by a red line. In a double dot system, charge stability diagram (hexagonal patterns) is described by $\Delta V_{g1(2)}^{\mathrm{m}}/\Delta V_{g1(2)} = C_{\mathrm{m}}/C_{2(1)}$, where the $\Delta V_{g1}^{\mathrm{m}}$ is the Coulomb peak splitting in $\Delta V_{g1(2)}$, where $\Delta V_{g1(2)}$ the Coulomb peak spacing in $V_{g1(2)}$, $C_{2(1)}$ the sum of all capacitances attached to the dot2(1), C_{m} coupling capacitance between dot1 and dot2 [20]. As the vertical distance between the tip and sample surface is much smaller than the lateral distance between the scanning positions to SWCNT–QD, an approximation of $C_{\mathrm{dot-tip}}(r) \propto 1/\left|\boldsymbol{r}_{\mathrm{tip}} - \boldsymbol{r}_{\mathrm{dot}}\right|$ was made. Thus, $\Delta r_{1(2)}^{\mathrm{m}}/\Delta r_{1(2)} = C_{\mathrm{m}}/C_{2(1)}$ was used in the following analysis of the scanning gate images. In several hexagonal patterns shown in figure 4(a), the $\Delta r_{1(2)}^{\mathrm{m}}$ and $\Delta r_{1(2)}$ were measured along the diameter of the different set of rings (green lines for dot1 and black for dot2), as demonstrated in figure 4(a). Consequently, the value of C_{m}/C_1 is found to be in the range of $0.21 \sim 0.27$ and C_{m}/C_2 in the range of $0.23 \sim 0.28$. If we simply neglect the contribution of inter-dot conductance (tunnel coupling), the magnitude of the coupling impedance, $|Z| = h(C_1C_2/C_{\mathrm{m}}^2 - 1)/(2\pi e^2)$, is $\sim 2.39\ h/e^2$ where h is Planck's constant [23].

The shape of these hexagonal patterns also changed with increasing V_{bg}. One of these overlap regions was tracked, and is pointed out by the end of the red arrow in figures 4(b)–(i). While from figures 4(b)–(e), the conductance rings still exhibit honeycomb patterns, with further increasing V_{bg}, some honeycomb patterns are distorted and some sections of the two rings merged into one as shown in figures 4(f)–(i). This indicates that the quantum mechanical tunnel coupling between the dots become so large that two dots merge into one large dot [25, 26]. The increased tunnel coupling can be attributed to the change in the QD confinement potential caused by the backgate bias voltage. The fluctuation of local charging sites in SiO_2 layer induced by the backgate may also contribute to the changes of the disorder potential, which is the origin of the QD confinement potential [27, 28]. When the confinement potential becomes weak, corresponding lowering the effective tunnel barrier between these two QDs, two QDs start to merge into one. Note that, in this case, it is not the filling of the QD that causes the increased tunnel coupling [29] as it did not change much as can be seen from figure 4.

In order to further understand the performance of the AFM tip as a movable gate, the conductance ring in the same spatial region has also been measured by varying V_{tip} from −2.225 to −2.1 V (step by 25 mV) while keeping $V_{\mathrm{bg}} = -38$ mV, as shown in figures 5(a)–(f). With increasing V_{tip}, the conductance rings slightly shrink towards the center of the dot, exhibiting similar tendency as the modulation of V_{bg}. However, we did not observe the similar distortion of

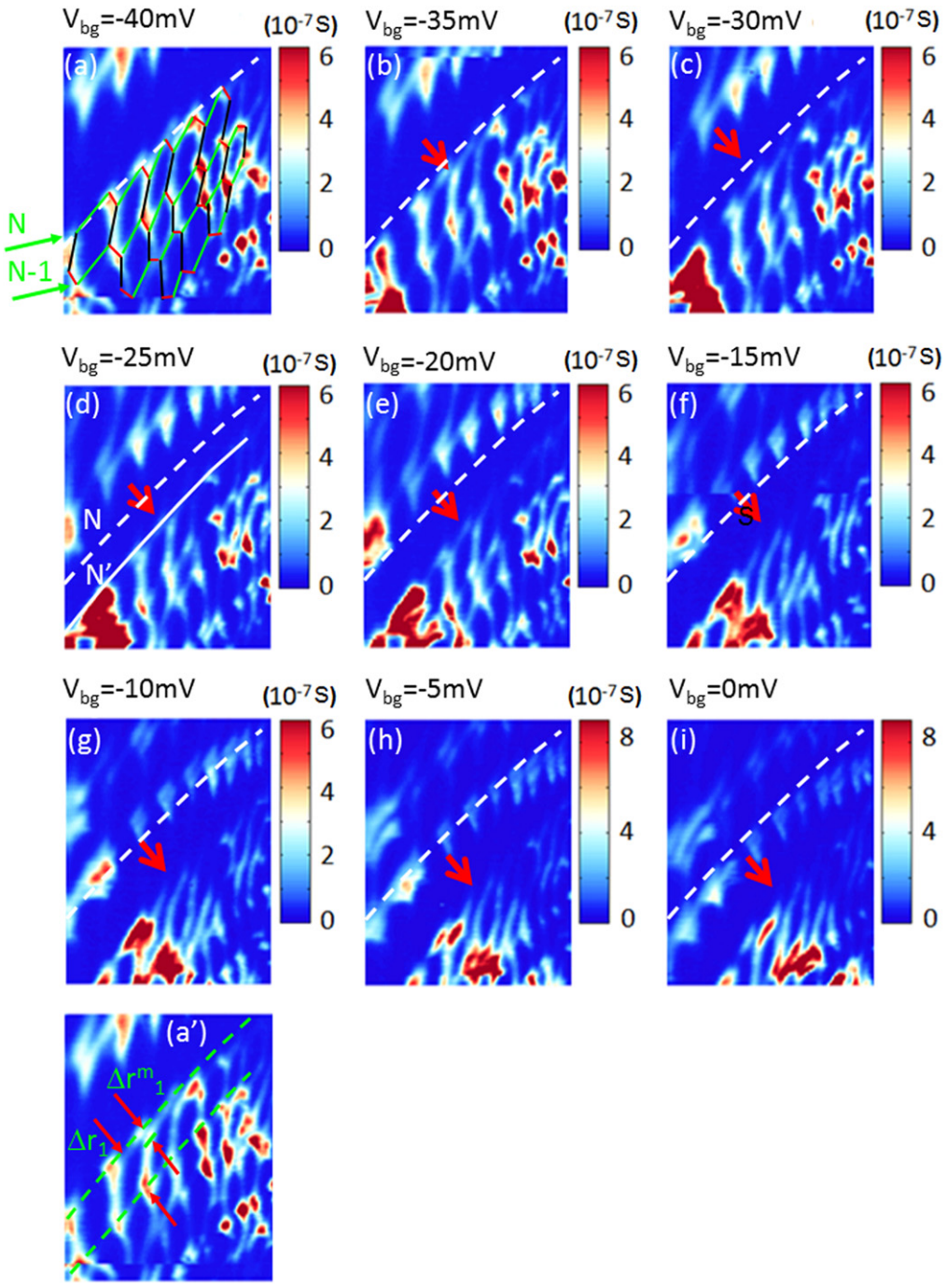

Figure 4. (a)–(i) Conductance images of the SWCNT taken at different backgate bias voltages, V_{bg}. The V_{bg} was varied from −40 to 0 mV with a step of 5 mV. $V_{ds} = 4$ mV and $V_{tip} = -2.1$ V were kept constant during the measurement. The tip scanning range was within green rectangle, marked in figure 3. The overlapping two sets of rings form hexagon patterns. The conductance rings of dot1 and dot2 are marked in green and black lines, respectively. Two of these conductance rings of dot1 are marked *N*th and *N*-1th. In order to make a position reference, the position of the initial *N*th conductance ring at $V_{bg} = -40$ mV was marked with white dash line from (a) to (i). With increasing V_{bg}, the *Nth* conductance ring moves towards the *N*-1th ring. When $V_{bg} = -25$ mV, the *N*th conductance ring moves from the white dashed line to the solid white line marked as *N* which was the previous position of the *N*-1th ring in figure 4(a), as shown in figure 4(d). (a) Shows how the values of Δr_1^m and Δr_1 were obtained from the conductance image in (a).

conductance rings which have been observed by modulation of V_{bg}. In order to make comparison between C_{bg} and $C_{dot-tip}$, the motion of one conductance ring was tracked by changing V_{bg} or V_{tip}. As shown in figures 4(a)–(d), values of V_{bg} are varied from −40 to −25 mV while keeping $V_{tip} = -2.1$ V constant, which cause *N*th conductance ring to move towards the center by one ring spacing. As shown in figure 4(d), the *N*th conductance ring almost reaches the position of *N*-1th conductance ring in figure 4(a) at $V_{bg} = -25$ mV. Thus, we can conclude that 15 mV is needed to remove one electron

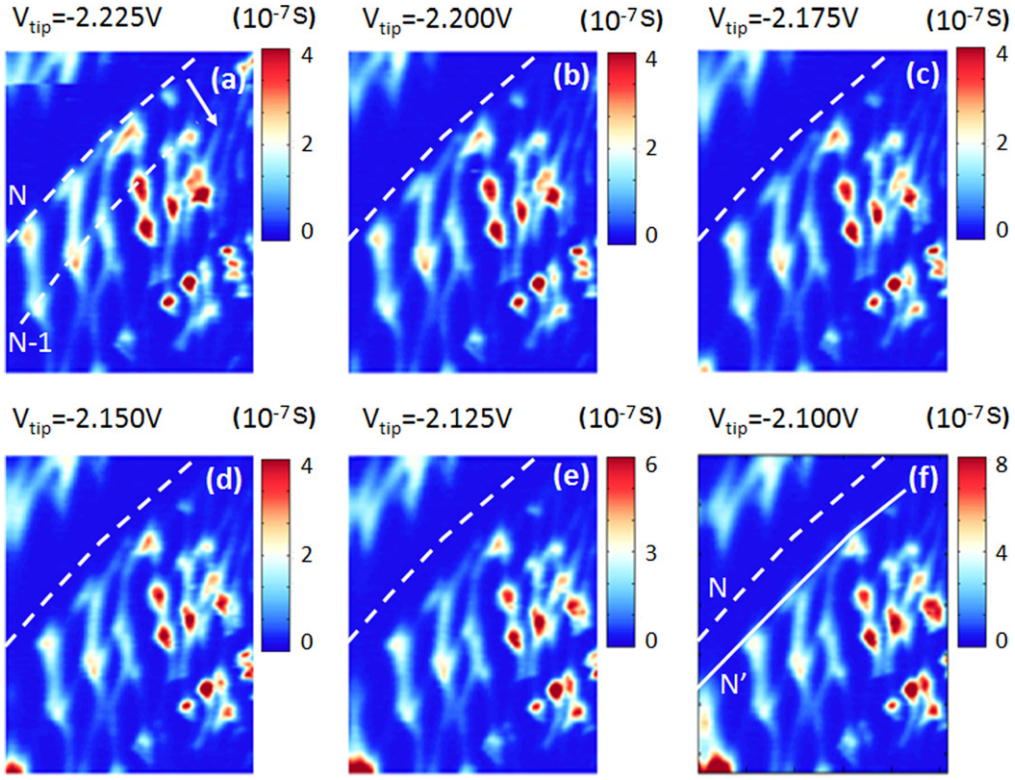

Figure 5. (a)–(f) Conductance images taken at different tip bias voltages, V_{tip}. The V_{tip} was varied from −2.225 to −2.100 V with a step of 25 mV with keeping $V_{bg} = -38$ mV constant. We still keep on tracking the same *N*th and *N*-1th conductance rings which are marked on figure 4(a). With increasing V_{tip}, the *N*th conductance rings moves slightly towards to the *N*-1th conductance rings. However, when $V_{tip} = -2.1$ V, the *N*th conductance rings, which are marked in a solid white line as *N*, are still far from the position of *N*-1th conductance rings in figure 5(a), as shown in figure 5(f).

from dot. However, when V_{tip} is varied from −2.225 to −2.1 V, no conductance ring moves over one ring spacing as shown in figures 5(a)–(f). In other words, it means the $C_{dot-tip}$ is much smaller than C_{bg}, because $e = C_{dot-tip}\Delta V_{tip} = C_{bg}\Delta V_{bg}$ [9]. Based on above measurement, the upper bound of the ratio $C_{dot-tip}/C_{bg}$ is estimated to be 0.12. This is because the AFM tip is far from the SWCNT-dots which makes the $C_{dot-tip}$ relatively small.

3.3. Observation of peak splitting

For coupled double dots, the split of CB conductance peaks can be caused by capacitive coupling and tunnel coupling [30]. Classical interdot capacitive coupling which reduces the energy of polarized charge configuration leads to conductance peak splitting. However, it requires that the interdot coupling capacitance increase strongly while the interdot tunnel conductance remains negligible [31–33]. When interdot tunnel conductance is no longer negligible, quantum fluctuations between dots also cause peak splitting [31, 34]. In both cases, the separation of the peak splitting indicates the coupling strength between these two dots because the separation of peak splitting is proportional to the coupling strength regardless of coupling mechanism.

In the SGM measurement, the inter-dot coupling phenomenon can be observed by varying V_{tip} or tip position. Here, we still focus on the double dot system where there are only two sets of overlapping rings. One of the typical conductance image was taken by biasing $V_{tip} = -2$ V, $V_{bg} = -72$ mV and scanning tip in a range of $\Delta X_{tip} = 150$ nm and $\Delta Y_{tip} = 150$ nm, as shown in figure 6. Here, the scanned region is different from the region shown in figure 4 and figure 5. Four different scanned regions have been marked (A)–(D) in figure 6. In the region (A), two conductance rings which belong to two different SWCNT-dots starts to bend and split. In contrast to the region (A), in the region (B)–(D), two conductance rings just overlap and do not clearly split in the overlap region. Figure 7 shows the $I_{ds} - V_{tip}$ curves measured at the positions marked as the black point in each region (A)–(D) in figure 6 by biasing $V_{ds} = 5$ mV, $V_{bg} = -75$ mV and sweeping V_{tip} from −2.2 to −1.8 V. We focus on these Coulomb peaks around $V_{tip} = -2$ V, as the conductance image in the figure 6 was measured by biasing $V_{tip} = -2$ V. At position (A), at around $V_{tip} = -2$ V, single-electron transport is Coulomb blockaded as there is no Coulomb peak at this voltage. It is consistent that there is no conductance at the black point position in the conductance image, which indicates the energy levels of the double-dots do not align in the transport window. However, in the position (B)–(C), the Coulomb peaks at around $V_{tip} = -2$ V exhibit the weakly split peaks which indicate the weaker inter-dot coupling, as shown in figure 7(B)–(C). In

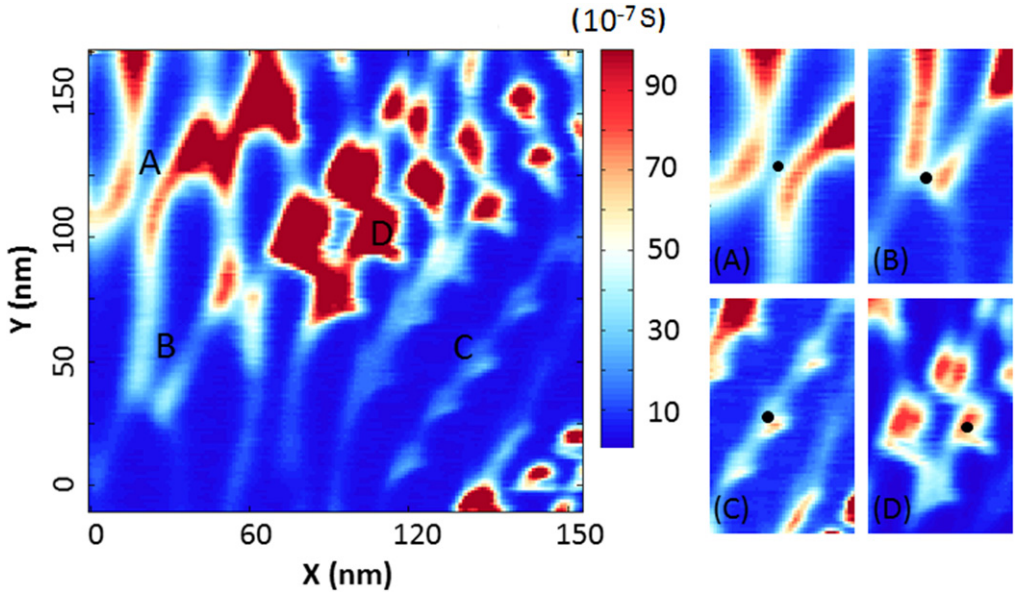

Figure 6. (Left) Conductance image taken at $V_{tip} = -2$ V, $V_{bg} = -72$ mV. (Right) (A)–(D) zoomed in images of the positions A–B indicated in the left image, respectively.

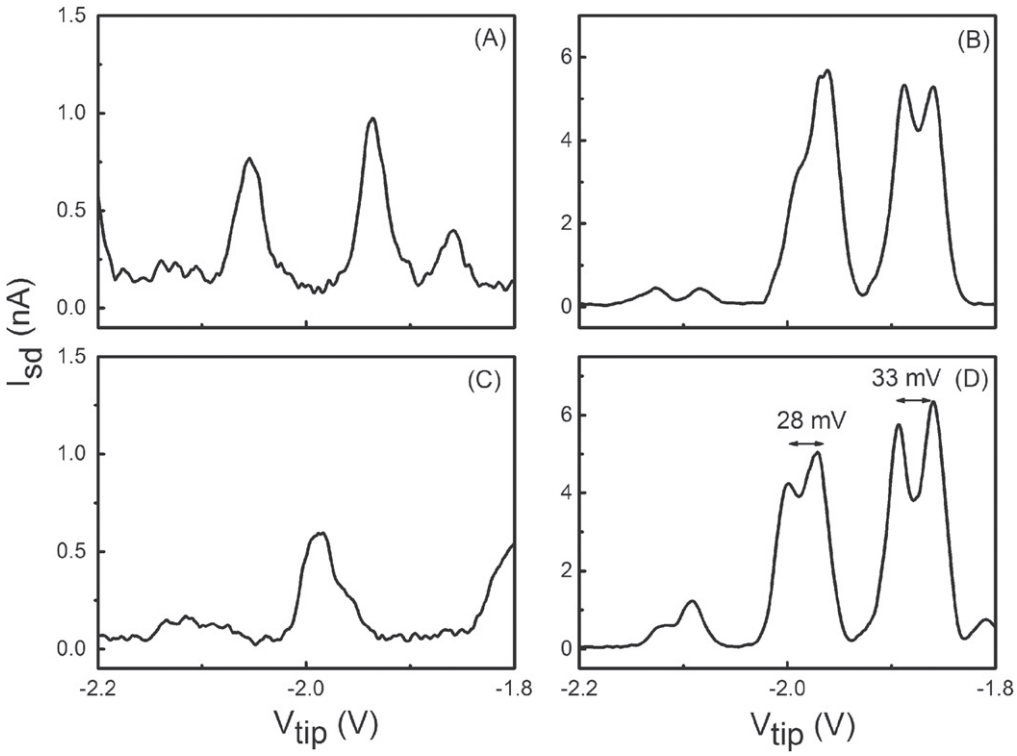

Figure 7. $V_{tip} - I_{ds}$ characteristics measured by locating tip at position (A)–(D) marked as red points in figure 6. Here, $V_{tip}-I_{ds}$ characteristics were obtained by biasing $V_{ds} = 5$ mV, $V_{bg} = -75$ mV and sweeping V_{tip} from −2.2 to −1.8 V.

position (D), the peak clearly splits into two peaks. The split peak separation is 28 mV around $V_{tip} = -2$ V and 33 mV around $V_{tip} = -1.9$ V, which is due to the increases of the inter-dot coupling effects [34]. However, from SGM images, it is difficult to determine the mechanism of inter-dot interactions by directly measuring the inter-dot conductance as previous reports [25, 35] because the stability diagram (SGM images) obtained with SGM technique is more complex than typical stability diagram obtained by sweeping gate bias voltages. In order to verify the inter-dot coupling mechanism for defect-induced tunnel barriers in SWCNT–QDs, further investigation is still required.

4. Conclusion

Two coupled SWCNT QDs in multiple-QD systems have been characterized by taking advantage of low temperature SGM measurement technique. The conductance images of the SWCNT channel exhibit several sets of conductance rings, which indicate the locations of these multiple-QDs along the SWCNT. The modulation of single-electron transport in SWCNT double QDs can be achieved by changing tip position and V_{tip}. The typical hexagonal patterns of coupled double dots have been clearly observed in conductance images. The capacitance between AFM-tip and SWCNT-dots was less than 12% of the backgate capacitance. Based on conductance image of coupled two dots, the values of coupling capacitance between two SWCNT-dots over total capacitance of each dot were also evaluated to be $C_m/C_1 = 0.21 \sim 0.27$ and $C_m/C_2 = 0.23 \sim 0.28$, respectively. In addition, the typical inter-dot coupling phenomenon, Coulomb peak splitting, also has been observed by varying the AFM tip position. The measurement results demonstrate the advantages of low temperature of SGM measurement technique.

Acknowledgments

Xin ZHOU was supported by the Special Postdoctoral Research Program of RIKEN and this research was also supported by NanoQuebec.

References

[1] Kuemmeth F, Churchill H O, Herring P K and Marcus C M 2002 *Mater. Today* **13** 18
[2] Katsnelson M I and Geim A K 2008 *Phil. Trans. R. Soc.* A 366
[3] Cobden D H, Bockrath M, McEuen P L, Rinzler A G and Smalley R E 1998 *Phys. Rev. Lett.* **81** 681
[4] Nygard J, Cobden D H and Lindelof P E 2000 *Nature* **408** 342
[5] Jarillo-Herrero P, Sapmaz S, Dekker C, Kouwenhoven L P and van der Zant H S J 2004 *Nature* **429** 389
[6] Biercuk M J, Ilani S, Marcus C M and McEuen P L 2008 *Carbon Nanotubes* (*Topics in Applied Physics* vol 111) (Berlin: Springer) p 455
[7] Bleszynski-Jayich A C, Froberg L E, Bjork M T, Trodahl H J, Samuelson L and Westervelt R M 2008 *Phys. Rev.* B **77** 245324
[8] Woodside M T and McEuen P L 2002 *Science* **296** 1098
[9] Boyd E E, Storm K, Storm L, Samuelson L and Westervelt R M 2011 *Nanotechnology* **22** 185201
[10] Tabata H, Shimizu M and Ishibashi K 2009 *Appl. Phys. Lett.* **95** 113107
[11] Zhou X and Ishibashi K 2012 *Appl. Phys. Lett.* **101** 123506
[12] Hedberg J A, Lal A, Miyahara Y, Grutter P, Gervais G, Hilke M, Pfeiffer L and West K W 2010 *Appl. Phys. Lett.* **97** 143107
Hedberg J A 2011 *PhD Thesis* McGill University
[13] Zahl P, Bierkandt M, Shrder S and Klust A 2003 *Rev. Sci. Instrum.* **74** 1222
[14] Kouwenhoven L P, van der Vaart N C, Johnson A T, Kool W, Harmans C J P M, Williamson J G, Staring A A M and Foxon C T 1991 *Z. Phys.* B **85** 367
[15] Ishibashi K, Moriyama S, Tsuya D, Fuse T and Suzuki M 2006 *J. Vac. Sci. Technol.* A **24** 1349
[16] Bockrath M, Liang W, Bozovic D, Hafner J H, Lieber C M, Tinkham M and Park H 2001 *Science* **291** 283
[17] Yao Z, Dekker C and Avouris P 2001 ed M S Dresselhaus, G Dresselhaus and Ph Avouris Electrical transport through single-wall carbon nanotubes *Topics in Applied Physics* vol 80 (Berlin: Springer) p 147
[18] Fallahi P, Bleszynski A C, Westervelt R M, Huang J, Walls J D, Heller E J, Hanson M and Gossard A C 2005 *Nano Lett.* **5** 223
[19] Bleszynski A C, Zwanenburg F A, 1Westervelt R M, Roest A L, Bakkers E P A M and Kouwenhoven L P 2007 *Nano Lett.* **7** 2559
[20] Bleszynski-Jayich A C, Fröberg L E, Björk M T, Trodahl H J, Samuelson L and Westervelt R M 2008 *Phys. Rev.* B **77** 245327
[21] van der Wiel W G, Franceschi S D, Elzerman J M, Fujisawa T, Tarucha S and Kouwenhoven L P 2003 *Rev. Mod. Phys.* **75** 1
[22] Schnez S, Guttinger J, Stampfer C, Ensslin K and Ihn T 2011 *New J. Phys.* **13** 053013
[23] Huefner M, Kueng B, Schnez S, Ensslin K and Ihn T 2011 *Phys. Rev.* B **83** 235326
[24] Brink M 2007 Imaging single-electron charging in nanostructures by low-temperature scanning force microscopy *PhD Thesis* Cornell University
[25] Livermore C, Crouch C H, Westervelt R M, Campman K L and Gossard A C 1996 *Science* **274** 1332
[26] Mason N, Biercuk M J and Marcus C M 2004 *Science* **303** 655
[27] Waugh F R, Berry M J, Crouch C H, Livermore C, Mar D J, Westervelt R M, Campman K L and Gossard A C 1996 *Phys. Rev.* B **53** 1413
[28] Staring A A M, van Houten H, Beenakker C W J and Foxon C T 1992 *Phys. Rev.* B **45** 9222
[29] Brodsky M, Zhitenev N B, Ashoori R C, Pfeiffer L N and West K W 2000 *Phys. Rev. Lett.* **85** 2356
[30] Ruzin I M, Chandrasekhar V, Levin E I and Glazman L I 1992 *Phys. Rev.* B **45** 13469
[31] Waugh F R, Berry M J, Crouch C H, Livermore C, Mar D J and Westervelt R M 1996 *Phys. Rev.* B **53** 1413
[32] Glazman L I and Chandrasekhar V 1992 *Europhys. Lett.* **19** 623
[33] Ruzin I M, Chandrasekhar V, Levin E I and Glazman L I 1992 *Phys. Rev.* B **45** 469
[34] Waugh F R, Berry M J, Mar D J and Westervelt R M 1995 *Phys. Rev. Lett.* **75** 705
[35] DiCarlo L, Lynch H J, Johnson A C, Childress L I, Crockett K, Marcus C M, Hanson M P and Gossard A C 2004 *Phys. Rev. Lett.* **92** 226801